

SUPPORTING INFORMATION

Highly flexible biodegradable cellulose nanofiber/graphene heat spreader films with improved mechanical property and enhanced thermal conductivity

Yapeng Chen ^{a,b}, Xiao Hou ^a, Ruiyang Kang ^a, Yun Liang ^{a,b}, Liangchao Guo ^a, Wen Dai ^{a,b}, Kazuhito Nishimura ^c, Cheng-Te Lin ^{a*}, Nan Jiang ^{a*}, Jinhong Yu ^{a,b*}

^a *Key Laboratory of Marine Materials and Related Technologies, Zhejiang Key Laboratory of Marine Materials and Protective Technologies, Ningbo Institute of Materials Technology and Engineering, Chinese Academy of Sciences, Ningbo 315201, China*

^b *University of Chinese Academy of Sciences, 19 A Yuquan Rd., Shijingshan District, Beijing 100049, China.*

^c *Advanced Nano-processing Engineering Lab, Mechanical Systems Engineering, Kogakuin University, Kochi, 780-0805, Japan.*

****Corresponding author, Electronic mail: linzhengde@nimte.ac.cn; jiangnan@nimte.ac.cn; yujinhong@nimte.ac.cn.***

SUPPLEMENT

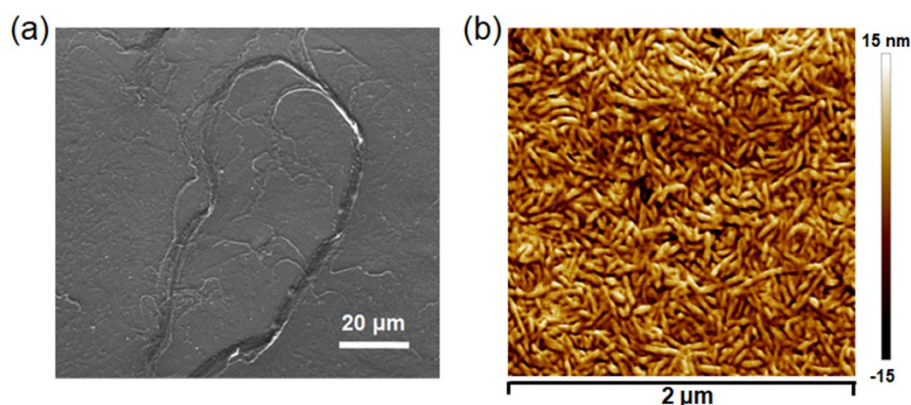


Fig. S1 (a) SEM image of cellulose nanofibers. **(b)** AFM tapping mode phase image of cellulose nanofibers on silica.

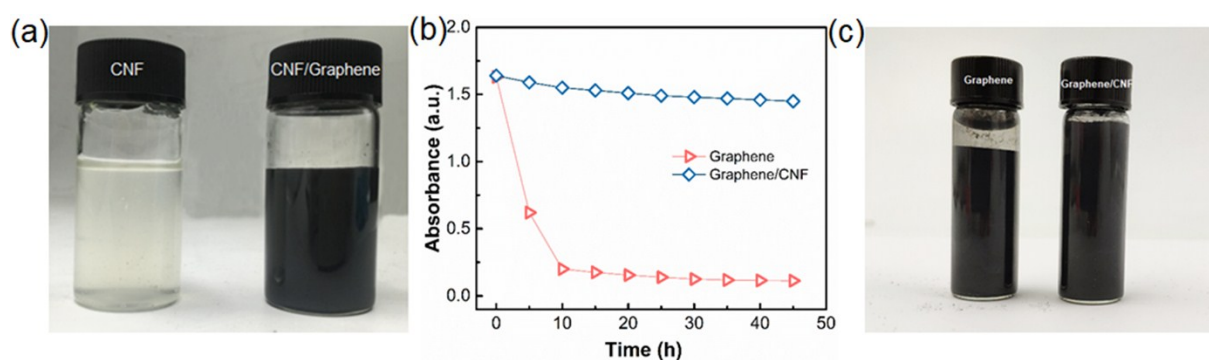


Fig. S2 (a) Digital photograph of cellulose nanofiber solution and 50 graphene/cellulose nanofiber dispersion (CNF: graphene = 1: 1). **(b)** Optical absorption as a function of time for graphene dispersion (0.1 mg/ml) and graphene/CNF dispersion (0.1 mg/ml, graphene: CNF = 9:1). **(c)** Digital picture of graphene (left, 5 mg/ml) and graphene/CNF dispersion (right, 5 mg/ml and graphene: CNF = 9:1) after standing 48 h.

Fig. S2 (a) shows the photograph of cellulose nanofiber solution and graphene/cellulose nanofiber solution with 50 wt% graphene. Graphene/cellulose nanofiber solution with 50 wt% graphene almost no change at all after one month, which exhibited excellent stability. As can be seen in **Fig. S2 (b)** the absorbance of graphene dispersion reduced to 0.2 after only 10 h, and the absorbance of graphene/CNF reduced slightly after 45 h. **Fig. S2 (b)** exhibited the digital picture of graphene and graphene/CNF dispersion (mass ratio of graphene and CNF is 9:1) at high concentration (5 mg/ml) after standing 48 h. As can be seen in **Fig. S2 (c)**, graphene dispersion revealed obviously precipitation and graphene/CNF dispersion still shown great dispersibility. Comparing with graphene dispersion, the introduction of CNF could greatly improve the dispersibility and stability of graphene in water at

whether high (5 mg/ml) or low (0.1 mg/ml) graphene concentration.

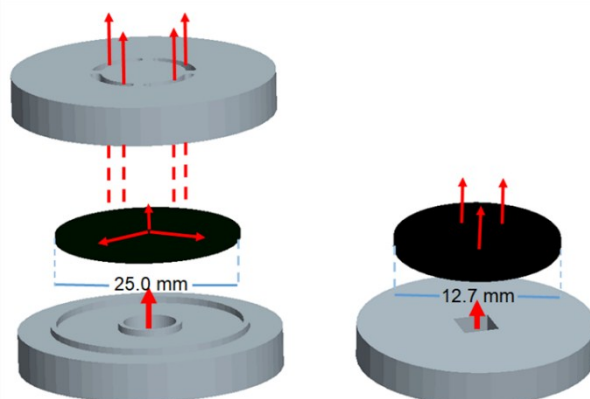


Fig. S3 schematic of the mold for characterize in-plane (left), and through-plane thermal diffusivity (right).

The in-plane sample holder is designed so that the position for the laser energy input on the bottom side of the sample and the position for measuring the temperature increase on the top side of the sample (laser energy output) are located at different lateral positions. Thus the measured temperature increase of the sample shows the thermal diffusivity in the radial direction (in-plane). Meanwhile, the through-plane thermal conductivities were measured by the round holder with a 12.7 mm diameter, as shown in the right of **Fig. S3**. Laser system flash a pulse and illuminate the bottom surface of samples. After absorbing light, the laser energy quickly passed to the top surface. The infrared detector that located above the sample can measure temperature variation and obtain the curve of temperature and time.



Fig. S4 Digital photo of the CNFG-50 composite film.

The cellulose nanofiber/graphene films with 50 wt% graphene loading shows excellent flexibility as

can be seen in Fig. S4.

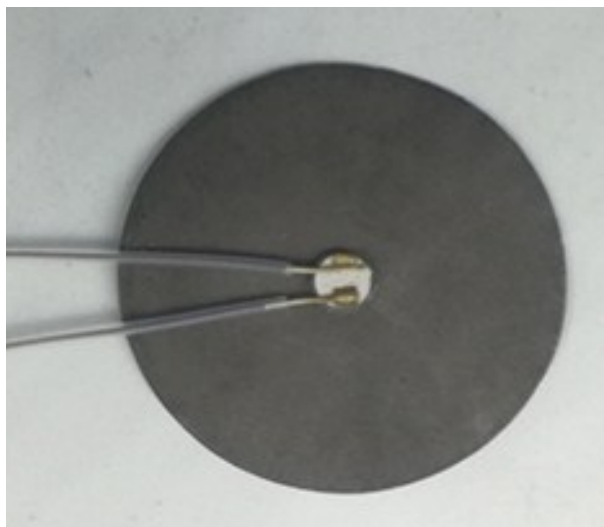


Fig. S5 Digital photograph of Al₂O₃ heater stucked on the sample with thermal conductive silicon.

As can be seen in Fig. S5, the Al₂O₃ heater was adhered to the underside of the sample. IR camera was used to record the surface temperature of the sample under 20 W heating power.

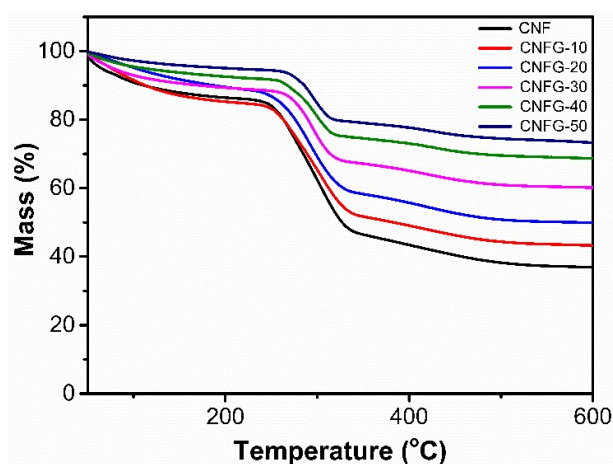


Fig. S6 Thermogravimetric analysis (TGA) of neat CNF and CNFG composite films.

Fig. S6 exhibits the TGA curves of neat CNF and CNFG composites under N₂ atmosphere. As can be seen in Fig. S6, graphene could enhance the thermal stability of cellulose nanofiber, the degradation temperature improved over 20 °C with 50 wt% graphene loading.

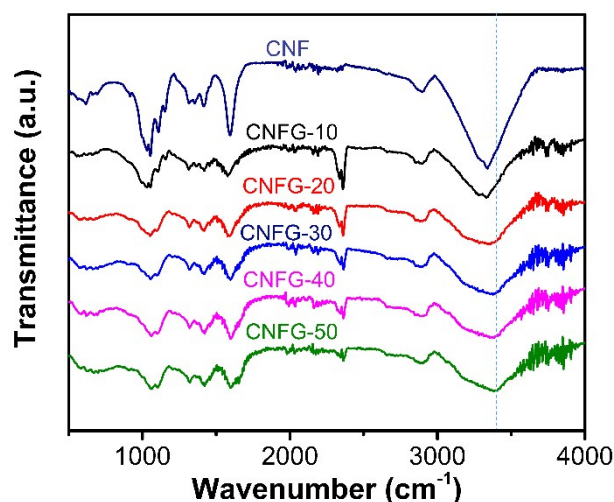


Fig. S7 FT-IR spectra of neat CNF, CNFG-10, CNFG-20, CNFG-30, CNFG-40 and CNFG-50.

As can be seen in **Fig. S7**, compared with pure CNF, the FT-IR spectra of CNFG with different graphene loading showed a shift to higher wavenumbers of the -OH peak region around 3440 cm^{-1} and -C-OH peak region around 1060 cm^{-1} , which are corresponding to -OH stretching from inter and intramolecular hydrogen bonds. Meanwhile, with the increase of graphene content, FT-IR spectra exhibited greater shift.

Table S1 Comparison of in-plane thermal conductivity of our CNFG and reported cellulose based composites.

Filler	Fraction	TC (W/mK)	Ref.
Laser-reduced GO	0.31 wt%	10.72	2018 ¹
Graphene	3 wt%	0.72	2017 ²
Graphene	90 wt%	240.5	2017 ³
Graphene	6 wt%	9.0	2017 ⁴
Graphene	10 wt%	6.75	2017 ⁵
Reduced GO	50 wt%	1.59	2017 ⁶
Reduced GO	1 wt%	12.6	2017 ⁷
Graphite nanoplatelets	75 wt%	59.46	2016 ⁸
Ag decorated boron nitride nanosheets	28.6 vol%	65.7	2017 ⁹
Functionalized Boron nitride nanosheets	70 wt%	30.25	2017 ¹⁰
Ag deposited SiC nanowires	50 vol%	33.97	2016 ¹¹
Reduced GO	30 wt%	6.168	2016 ¹²
Graphene	15 wt%	41	2015 ¹³

Boron nitride nanosheets	50 wt%	145.7	2014 ¹⁴
Graphene	50 wt%	164.7	This work

Note: [TC] Thermal conductivity; [Ref.] reference.

References

1. T. L. Zhou, H. Wei, H. P. Tan, X. Wang, H. B. Zeng, X. H. Liu, S. Nagao, H. Koga, M. Nogi, T. Sugahara and K. Suganuma, *2D Mater.*, 2018, **5**, 035013.
2. L. Chen, X. S. Hou, N. Song, L. Y. Shi and P. Ding, *Compos. Pt. A-Appl. Sci. Manuf.*, 2018, **107**, 189-196.
3. W. Yang, Y. Zhang, T. Liu, R. Huang, S. Chai, F. Chen and Q. Fu, *ACS Sustain. Chem. Eng.*, 2017, **5**, 9102-9113.
4. N. Song, X. S. Hou, L. Chen, S. Q. Cui, L. Y. Shi and P. Ding, *ACS Appl. Mater. Interfaces*, 2017, **9**, 17914-17922.
5. N. Song, S. Q. Cui, D. J. Jiao, X. S. Hou, P. Ding and L. Y. Shi, *Carbon*, 2017, **115**, 338-346.
6. W. X. Yang, Z. D. Zhao, K. Wu, R. Huang, T. Y. Liu, H. Jiang, F. Chen and Q. Fu, *J. Mater. Chem. C*, 2017, **5**, 3748-3756.
7. N. Song, D. J. Jiao, S. Q. Cui, X. S. Hou, P. Ding and L. Y. Shi, *ACS Appl. Mater. Interfaces*, 2017, **9**, 2924-2932.
8. G. H. Li, X. J. Tian, X. W. Xu, C. Zhou, J. Y. Wu, Q. Li, L. Q. Zhang, F. Yang and Y. F. Li, *Compos. Sci. Technol.*, 2017, **138**, 179-185.
9. J. J. Sun, Y. M. Yao, X. L. Zeng, G. R. Pan, J. T. Hu, Y. Huang, R. Sun, J. B. Xu and C. P. Wong, *Adv. Mater. Interfaces*, 2017, **4**, 1700563.
10. K. Wu, J. C. Fang, J. R. Ma, R. Huang, S. G. Chai, F. Chen and Q. Fu, *ACS Appl. Mater. Interfaces*, 2017, **9**, 30035-30045.
11. B. B. Campos, L. Gelde, M. Algarra, J. da Silva, M. I. Vazquez and J. Benavente, *Carbohydr. Polym.*, 2016, **151**, 939-946.
12. N. Song, D. J. Jiao, P. Ding, S. Q. Cui, S. F. Tang and L. Y. Shi, *J. Mater. Chem. C*, 2016, **4**, 305-314.
13. F. Z. Wang, L. T. Drzal, Y. Qin and Z. X. Huang, *Compos. Pt. B-Eng.*, 2015, **79**, 521-529.
14. H. Zhu, Y. Li, Z. Fang, J. Xu, F. Cao, J. Wan, C. Preston, B. Yang and L. Hu, *ACS Nano*, 2014, **8**, 3606-3613.